AFRL-AFOSR-VA-TR-2015-0381

Fabrication and Electrical Characterization of Correlated Oxide Field Effect Switching Devices for High Speed Electronics

Shriram Ramanathan
HARVARD COLLEGE PRESIDENT & FELLOWS OF

11/19/2015
Final Report

DISTRIBUTION A: Distribution approved for public release.

Air Force Research Laboratory
AF Office Of Scientific Research (AFOSR)/ RTA1
Arlington, Virginia 22203
Air Force Materiel Command

REPORT DOCUMENTATION PAGE

Form Approved
OMB No. 0704-0188

The public reporting burden for this collection of information is estimated to average 1 hour per response, including the time for reviewing instructions, searching existing data sources, gathering and maintaining the data needed, and completing and reviewing the collection of information. Send comments regarding this burden estimate or any other aspect of this collection of information, including suggestions for reducing the burden, to Department of Defense, Washington Headquarters Services, Directorate for Information Operations and Reports (0704-0188), 1215 Jefferson Davis Highway, Suite 1204, Arlington, VA 22202-4302. Respondents should be aware that notwithstanding any other provision of law, no person shall be subject to any penalty for failing to comply with a collection of information if it does not display a currently valid OMB control number.
PLEASE DO NOT RETURN YOUR FORM TO THE ABOVE ADDRESS.

1. REPORT DATE *(DD-MM-YYYY)*	2. REPORT TYPE	3. DATES COVERED *(From - To)*
01/11/2015	Final	06/01/2012 to 07/31/2015

4. TITLE AND SUBTITLE
Fabrication and electrical characterization of correlated oxide field effect switching devices for high speed electronics

5a. CONTRACT NUMBER

5b. GRANT NUMBER
FA9550-12-1-0189

5c. PROGRAM ELEMENT NUMBER

6. AUTHOR(S)
Shriram Ramanathan

5d. PROJECT NUMBER

5e. TASK NUMBER

5f. WORK UNIT NUMBER

7. PERFORMING ORGANIZATION NAME(S) AND ADDRESS(ES)
School of Engineering and Applied Sciences
Harvard University
29 Oxford St, Pierce Hall, Cambridge, MA 02138

8. PERFORMING ORGANIZATION REPORT NUMBER

9. SPONSORING/MONITORING AGENCY NAME(S) AND ADDRESS(ES)
Air Force Office of Scientific Research
875 N. Randolph Street
Ste. 325
Arlington, VA 22203-1768

10. SPONSOR/MONITOR'S ACRONYM(S)

11. SPONSOR/MONITOR'S REPORT NUMBER(S)

12. DISTRIBUTION/AVAILABILITY STATEMENT
Distribution A

13. SUPPLEMENTARY NOTES
None

14. ABSTRACT
The electronic properties of thin film correlated oxides was investigated via electrical transport measurements and electronic structure studies. Microscopic connection between insulator-metal switching, orbital occupancy, electron-phonon interactions was emphasized. The response of correlated oxides to strong electric fields and their dynamics was investigated. A few different oxide systems were considered during the course of the study: they include VO2, SmNiO3, and NbO2. The common aspects of these materials include their thermal insulator-metal transition.

15. SUBJECT TERMS

16. SECURITY CLASSIFICATION OF:			17. LIMITATION OF ABSTRACT	18. NUMBER OF PAGES	19a. NAME OF RESPONSIBLE PERSON
a. REPORT	b. ABSTRACT	c. THIS PAGE			19b. TELEPHONE NUMBER *(Include area code)*
U	U	U	UU	14	

INSTRUCTIONS FOR COMPLETING SF 298

1. REPORT DATE. Full publication date, including day, month, if available. Must cite at least the year and be Year 2000 compliant, e.g. 30-06-1998; xx-06-1998; xx-xx-1998.

2. REPORT TYPE. State the type of report, such as final, technical, interim, memorandum, master's thesis, progress, quarterly, research, special, group study, etc.

3. DATE COVERED. Indicate the time during which the work was performed and the report was written, e.g., Jun 1997 - Jun 1998; 1-10 Jun 1996; May - Nov 1998; Nov 1998.

4. TITLE. Enter title and subtitle with volume number and part number, if applicable. On classified documents, enter the title classification in parentheses.

5a. CONTRACT NUMBER. Enter all contract numbers as they appear in the report, e.g. F33315-86-C-5169.

5b. GRANT NUMBER. Enter all grant numbers as they appear in the report. e.g. AFOSR-82-1234.

5c. PROGRAM ELEMENT NUMBER. Enter all program element numbers as they appear in the report, e.g. 61101A.

5e. TASK NUMBER. Enter all task numbers as they appear in the report, e.g. 05; RF0330201; T4112.

5f. WORK UNIT NUMBER. Enter all work unit numbers as they appear in the report, e.g. 001; AFAPL30480105.

6. AUTHOR(S). Enter name(s) of person(s) responsible for writing the report, performing the research, or credited with the content of the report. The form of entry is the last name, first name, middle initial, and additional qualifiers separated by commas, e.g. Smith, Richard, J, Jr.

7. PERFORMING ORGANIZATION NAME(S) AND ADDRESS(ES). Self-explanatory.

8. PERFORMING ORGANIZATION REPORT NUMBER. Enter all unique alphanumeric report numbers assigned by the performing organization, e.g. BRL-1234; AFWL-TR-85-4017-Vol-21-PT-2.

9. SPONSORING/MONITORING AGENCY NAME(S) AND ADDRESS(ES). Enter the name and address of the organization(s) financially responsible for and monitoring the work.

10. SPONSOR/MONITOR'S ACRONYM(S). Enter, if available, e.g. BRL, ARDEC, NADC.

11. SPONSOR/MONITOR'S REPORT NUMBER(S). Enter report number as assigned by the sponsoring/ monitoring agency, if available, e.g. BRL-TR-829; -215.

12. DISTRIBUTION/AVAILABILITY STATEMENT. Use agency-mandated availability statements to indicate the public availability or distribution limitations of the report. If additional limitations/ restrictions or special markings are indicated, follow agency authorization procedures, e.g. RD/FRD, PROPIN, ITAR, etc. Include copyright information.

13. SUPPLEMENTARY NOTES. Enter information not included elsewhere such as: prepared in cooperation with; translation of; report supersedes; old edition number, etc.

14. ABSTRACT. A brief (approximately 200 words) factual summary of the most significant information.

15. SUBJECT TERMS. Key words or phrases identifying major concepts in the report.

16. SECURITY CLASSIFICATION. Enter security classification in accordance with security classification regulations, e.g. U, C, S, etc. If this form contains classified information, stamp classification level on the top and bottom of this page.

17. LIMITATION OF ABSTRACT. This block must be completed to assign a distribution limitation to the abstract. Enter UU (Unclassified Unlimited) or SAR (Same as Report). An entry in this block is necessary if the abstract is to be limited.

DISTRIBUTION A: Distribution approved for public release

Title: Fabrication and electrical characterization of correlated oxide field effect switching devices for high speed electronics

PI: Shriram Ramanathan, Harvard University

AFOSR Grant FA9550-12-1-0189, (Program Manager: Dr. Ken Goretta)

Final Report

Report Summary

The electronic properties of thin film correlated oxides was investigated via electrical transport measurements and electronic structure studies. Microscopic connection between insulator-metal switching, orbital occupancy, electron-phonon interactions was emphasized. The response of correlated oxides to strong electric fields and their dynamics was investigated. A few different oxide systems were considered during the course of the study: they include ($3d^1$) VO_2, ($3d^7$) $SmNiO_3$ and ($4d^1$) NbO_2. The common aspects of these materials include their thermal insulator-metal transition. At the same time, the different crystal structure between the binary oxides and the perovskite nickelates and the nature of d-orbital filling leads to profound complexity in the electronic nature of the phase change. In the report below, particular emphasis on the orbital splitting effects and conductivity of NbO_2 is discussed in detail and compared with a model system of VO_2. Optical properties from 0.2 to 6.5 eV of epitaxial NbO_2 ($4d^1$ system) films in their insulating states were investigated by spectroscopic ellipsometry. We found a $d_{||}$-e_g^{π} orbital splitting energy of ~1.6 eV in NbO_2 compared to ~1.3 eV in VO_2. The edge of the O2*p*-like valence band is estimated to be 3.2 eV below the Fermi level through x-ray photoelectron spectroscopy measurements, suggesting that electrons from O2*p* states do not contribute to optical absorption below this energy.

I. INTRODUCTON

Metal-insulator transitions (MITs) in oxides are an intriguing problem from both a fundamental materials physics and an applied technology perspective [1]. Though the precise roles of electron correlations and lattice distortions on the phase transition remains an active area of research, many recent theoretical studies have suggested intimate interplay among the orbital splitting/polarization, correlation effects, and Peierls dimerization in the $3d^1$ system [2-6]. Occupied states have been probed by x-ray photoelectron spectroscopy (XPS) [7], and a rough structure of unoccupied 3*d*-like states have been deduced by O *K*-edge x-ray absorption measurements [8-10]. NbO_2, a $4d^1$ system, like VO_2 crystallizes in a distorted rutile-type structure with Nb dimers and undergoes a temperature-induced MIT, albeit at a considerably higher temperature of ~1083 K [11]. It is commonly accepted that because 4*d* orbital valence states are more dispersed in both space and energy, Mott physics is less important in 4*d* transition-metal oxides than in 3*d* ones. Along this line of reasoning, it is perhaps surprising that the insulating state of NbO_2 persists to higher temperatures than that of VO_2. A proposed explanation for this difference is that the Peierls effect in NbO_2 is stronger due to larger Nb metal-metal overlap of 4*d* orbitals, leading to greater orbital splitting between occupied $d_{||}$ states and the unoccupied e_g^{π} states [12]; however, given the many attempts to revise and improve theoretical and computational studies of VO_2 [2-5,13], the physical and electronic properties of NbO_2 also should be examined more thoroughly. Currently, there are few experimental studies that provide insight into the electronic structure of NbO_2.

There have been diffraction [14,15], calorimetry [16], electrical [11,17-19], and magnetic [19] studies on bulk NbO_2, which have shown that it transforms from a high-temperature rutile-structure metal to a low-temperature Nb-dimerized diamagnetic insulator at ~1083 K. Recently epitaxial NbO_2 thin films have been grown on (0001) Al_2O_3, (111) MgO, (111) $MgAl_2O_4$, and (111) perovskite oxide substrates [20,21]. The key to achieving epitaxy of (100) rutile-type compounds is exploiting substrate surfaces with eutactic planes [22].

DISTRIBUTION A: Distribution approved for public release

II. EXPERIMENTAL DETAILS

Epitaxial NbO_2 films were grown on (0001) Al_2O_3 by DC reactive sputtering of a Nb metal target at 650 ^oC, 200 W, 10 mTorr, 7.5 sccm O_2, and 42.5 sccm Ar. An epitaxial (010) VO_2 film was grown on (0001) Al_2O_3 by RF sputtering a V_2O_5 ceramic target at 450 ^oC, 150 W, 5 mTorr, 1.3 sccm O_2, and 48.7 sccm Ar. Deposition conditions were optimized to both achieve stoichiometric phases as well as film smoothness for reliable ellipsometry measurements. X-ray reflectivity was used to measure the film thickness, and x-ray diffraction was used for phase and orientation determination. Raman spectroscopy was performed in a confocal microscope using a 532 nm laser source; a filter prevents the collection of signal <170 cm^{-1}. Electrical transport measurements were performed in the van der Pauw geometry; contact pads of 5 nm of Ti and then 50 nm of Au were sputtered on the films. *Ex-situ* XPS scans were taken with Al *K*□ radiation and with an electron flood gun that prevents charging, and the samples were grounded to the spectrometer. The energy scale of the XPS data is referenced so that Au4$f_{7/2}$ peak is at 84.0 eV.

Spectroscopic ellipsometry measurements were taken at incident angles of 50^o and 70^o with respect to the plane normal. These experiments were performed by collaborator at Woollam Inc. By checking data taken at different in-plane rotations, we confirmed that in-plane anisotropy is not present into our measurements, which is expected because the rutile-type thin films grow with rotational variants and hence 3-fold in-plane global rotational symmetry [20,22]. Furthermore, though our rutile-type films are oriented out-of-plane, we were able to fit all of our data at both incident angles assuming isotropic optical constants, which may be due to the small path length difference between the *p* and the *s* polarized light within the thin films. Thus, our measurements are not sensitive to the possible crystal optical anisotropy of VO_2 and NbO_2. Our optical conductivity spectra should be thought of as polarization averaged. All data sets were fitted both point by point and also separately with analytical oscillators. Point-by-point fitting has the advantage that it does not impose a functional form to the dielectric functions, but analytical oscillator fitting has the advantage that the resultant dielectric functions are ensured to satisfy the Kramers-Kronig relations. Both types of fits for all of our data sets presented here gave quantitatively comparable results. We strove to use the minimum number of oscillators while maintaining high fidelity of fitting, so that fitted parameters of different samples can be fairly compared, but the choice of oscillators is not unique. We used a collection of Lorentz and Tauc-Lorentz oscillators; the imaginary part of the dielectric function has a functional form with respect to energy *E* of:

$$\varepsilon_2 = \sum_i \frac{A_i B_i^2 E_i E}{\left(E_i^2 - E^2\right)^2 + B_i^2 E^2} + \sum_j \frac{A_j C_j E_j \left(E - E_{gj}\right)}{\left(E^2 - E_j^2\right)^2 + C_j^2 E^2} \frac{\Theta\left(E - E_{gj}\right)}{E}$$

where □ is the Heavyside step function. $A_{i(j)}$, $B_{i(j)}$, $E_{i(j)}$, E_{gj}, and C_j are the fit parameters for the ith Lorentz oscillator and the jth Tauc-Lorentz oscillator.

III. RESULTS

The real optical conductivity of V1, N1, and N2 are shown in Figs. 1(a)-(c). Results of the point-by-point and oscillator fits are compared, and the contribution of each individual oscillator is also displayed. Fitted parameters are summarized in Table I. The lowest energy optical excitation feature can be fitted adequately mainly by a single Tauc-Lorentz oscillator. The center energy is 1.31 eV for V1 and 1.58 eV for both N1 and N2. Though N1 and N2 should be nominally the same in terms of deposition conditions, aside from a small difference in thickness, we can see that that higher-energy (>3.5 eV) features are different; in particular, N2 shows higher conductivity and more spectral features. Nevertheless, their low-energy spectra (<3.5 eV) are quite comparable, as captured by their respective Oscillators 1 and 3 in Table I.

Sum-rule analysis [Fig. 1(d)] can be performed on optical conductivity spectra to determine the effective number of electrons n_{eff} per formula unit of NbO_2 accounting for optical excitation from 0 to a cutoff energy of *E*.

DISTRIBUTION A: Distribution approved for public release

$$n_{eff}(E) = \frac{2m_0}{N\pi e^2\hbar}\int_0^E \sigma_1(E')dE'$$

where m_0 is the bare electron mass and N is the volume density of formula units of NbO_2 or VO_2.

X-ray diffraction scans of N1 and N2 reveal that the both of the films are (110)-oriented in using Miller indices of its room-temperature distorted $I4_1/a$ unit cell [15], which corresponds to the pseudorutile (100) orientation [Fig. 2(a)]. The out-of-plane spacings, pseudorutile *a* lattice parameters, of both samples are 4.835 Å, which is within the range of reported values of bulk crystals [15,23,24]. Note that the film peak of N1 is broader and slightly asymmetric. There is a weak second NbO_2 orientation in N2, but no other peaks for N1. We did, however, find slight differences in Raman peak positions, particularly for the mode near 390 cm^{-1}, as well as weaker signal for the mode at 272 cm^{-1} in N1 [Fig. 2(b)]. Moreover, the Raman peaks of N2 are more intense and sharper of those of N1. Therefore, the contrast between the optical conductivity of N1 and N2 may be due to minor differences in point defect concentrations and/or in residual thin-film strain within the NbO_2 phase.

XPS was employed to probe the energy positions of the occupied valence band states of V1, N1, and N2 [Fig. 3(a)]. There are two stark differences: (1) emission from occupied valence *d* electron states is maximized at 0.85 eV for VO_2 and ~1.25 eV for NbO_2 (1.3 eV for N1 and 1.2 for N2), and (2) the emission edge of O2*p*-like states are estimated to be ~2.0 eV for VO_2 and ~3.2 eV for NbO_2. Because the samples are grounded to the spectrometer, the binding energies should be interpreted as the energies with respect to their Fermi levels. Our XPS spectrum of V1 matches closely to that of Shin *et al*. [7] The O2*p* band energies of N1 and N2 closely resemble recent *in-situ* photoemission studies of epitaxial NbO_2 films on (111) perovskite substrates [21]. Since XPS is surface sensitive, and both VO_2 and NbO_2 are susceptible to surface oxidation to their highest oxides, the intensity for transition-metal valence *d* peak depends on the degree of surface oxidation in ambient conditions. For example, surface oxidation on N2 is more pronounced than on N1. Nevertheless, for seven different NbO_2 films measured, we find that though the relative intensity may differ, the position in energy of Nb4*d* valence peak does not change to within ±0.1 eV, which is roughly the resolution limit of the XPS system (data not shown). The same is true for the position of the O2*p*-like band. The higher oxide and NbO_2 differ mainly in 4*d* electron filling; thus despite some degree of surface oxidation, the valence band XPS nevertheless yields a good estimate of the O2*p* band position of NbO_2. A core-level Nb3*d* XPS scan of N2 illustrates there is in fact some unavoidable sample surface oxidation once the sample is exposed to the ambient, showing Nb^{5+} 3*d* doublets [Fig 3(b)]. Regardless, there is also a clear signature of Nb^{4+}. Core-level peak positions of N2 are listed in Table II, and they closely match reported values from bulk crystals [26,27]. After background subtraction, the Nb3*d* core-level XPS spectrum of N2 in Fig. 3(b) was fitted with two doublet pairs. Each pair corresponds to the spin-orbit-split $3d_{5/2}$ and $3d_{3/2}$ levels of two different Nb valence states, 5+ and 4+. For each pair, we constrained the relative integrated intensities between $3d_{5/2}$ and $3d_{3/2}$ to be 3:2 and possessing the same full-width at half maximum (FWHM) values. The FWHM value of fitted Nb^{4+} peaks was 1.28 eV and that of Nb^{5+} was 1.31 eV. The integrated intensity ratio between Nb^{4+} and Nb^{5+} was 31:69. However, we believe that the Nb^{5+} oxide is confined to the very surface, because in our experience, core-level Nb3*d* scans of even elemental Nb metal films show a comparable amount of Nb^{5+} signature due to surface oxidation in ambient conditions. Figure 3(c) reveals the activation energy for electrical conduction to be 0.16 eV for N1 and 0.135 eV for N2. The weaker temperature dependences exhibited by both samples at low temperatures may be indicative of hopping transport via defect states.

IV. DISCUSSION

Using Goodenough's nomenclature [28], the antibonding *d*-like states that partake in bonding with surrounding oxygen are $d_{||}$ and e_g (t_{2g} in octahedral symmetry), where $d_{||}$ refers to the orbitals that are also involved in direct metal-metal bonding. The two *d*-like orbitals that bond with oxygen are referred to as $d_{}$(e_g in octahedral symmetry). In the dimerized insulating states of both VO_2 and NbO_2,

DISTRIBUTION A: Distribution approved for public release

the $d_{||}$ further splits into $d_{||}$ metal bonding and $d_{||}^*$ metal antibonding states. For our discussion, we assume that the arrangement of lowest to highest energy orbitals is $d_{||} \rightarrow e_g^{\pi*} \rightarrow d_{||}^* \rightarrow d_{\pi}$, which is supported by a number of computational studies [2,12,29,30]. However, we do acknowledge there should be band overlap, particularly between the $e_g^{\pi*}$ and $d_{||}^*$ bands. For the purpose of our discussion, we will also assume that the lone *d* electron resides solely in the $d_{||}$ state, but note that computational studies typically do not yield full orbital polarization in the insulating states [2,3,12].

Because binding energy edge of the O2*p*-like states deduced by XPS [Fig. 3(a)] is ~3.2 eV for NbO_2 and ~2.0 eV for VO_2, we assume that excitation of the one 4*d* (3*d*) electron is mainly responsible for the optical conductivity below these energies for NbO_2 (VO_2). This assumption can be justified by the observation that n_{eff} is considerably less than 1 at the stated energies for each compound [Fig. 1(d)]. Table I shows that the center energies of Tauc-Lorentz oscillator used to fit the lowest energy absorption feature are 1.31 eV for V1 and 1.58 eV for N1 and N2. This center energy ranges from 1.56 to 1.67 eV for ten different NbO_2 thin films measured. In both experimental [31] and theoretical [32] studies of VO_2, similar optical excitation is thought to be indicative of a $d_{||} \rightarrow e_g^{\pi*}$ transition, representative of the essential orbital splitting that is required to stabilize the insulating state. Experimentally, reported peak energies range from 1.1 to 1.35 eV for VO_2 [31,33-36]. Therefore, we assign the peak energy of 1.58 eV in N1 and N2 to be representative of the $d_{||}$-$e_g^{\pi*}$ orbital splitting; the larger separation in NbO_2 appears to be consistent with its higher transition temperature.

The center energies of oscillators 1 in N1 and N2 are only slightly larger than the binding energy peak of the occupied $d_{||}$ band as determined by XPS, which suggests that the Fermi level is close to the conduction band edge and explains the small activation energy observed in electrical transport. Hence, the activation energy should not be interpreted as half of the band gap. In Jannick and Whitmore's electrical transport study of bulk ceramic NbO_2, they found a higher activation energy of ~0.45 eV [18]. Furthermore, we believe that the center energies of Oscillators 3 in N1 (2.96 eV) and N2 (2.97 eV) are representative of the $d_{||} \rightarrow d_{||}^*$ transition. This assignment is close to the separation concluded in DFT calculations based on the LDA approximation, but it should be noted that any possible correlation effects were not accounted for [12]. On the other hand, we also note that an older calculation of the joint density of states of NbO_2 performed by Posternak *et al*. does not show a distinct peak at ~3.0 eV [37]. From Jiang and Spence's O *K*-edge electron energy loss spectroscopy (EELS) studies of NbO_2 [38], they deduced that the octahedral crystal field splitting of *unoccupied* 4*d*-like π^* and σ^* antibonding states to be ~3.5 eV. We assume this value to be the approximate separation between the $e_g^{\pi*}$ and d_{π} states. Therefore, any possible excitation to the d_{π} states contributes minimally to that of the peak captured by Oscillator 3. Furthermore, considering the position of the O2*p* band as deduced by XPS, excitation of electrons from O2*p* states likewise should contribute insignificantly to the Oscillator 3 peaks of N1 and N2. Table I shows that Oscillator 3 of V1 peaks at 2.92 eV; however, in this sample, the origin is more difficult to isolate because O2*p* $\rightarrow$ $e_g^{\pi*}$ transitions contribute heavily at this energy range, as is suggested by previous studies [28,32,35] as well as by the lower O2*p* photoelectron band edge energy of V1 at 2.0 eV below the Fermi level [Fig. 3(a)]. In VO_2 thin films, Qazilbash *et al*. report an optical peak at 2.5 eV attributed to $d_{||} \rightarrow d_{||}^*$ transition [31], and Verleur *et al*. observe a peak at ~2.75 eV in bulk and ~3.0 eV in thin-film samples but did not assign them to any particular transition. Whether a discernable peak emerges in theoretical optical conductivity calculations of VO_2 depends on the model used and computational details [32].

For NbO_2 at photon energies >3.2 eV, it is clear that a combination of transitions from occupied O2*p* and $d_{||}$ states are involved, so we do not attempt to make any further assignments of optical features to specific transitions. If excitonic and other excited-state correlation effects can be ignored, Fig. 4 represents a rough schematic of the energy ordering of the different bands (orbitals) with respect to the Fermi level of our NbO_2 samples, as deduced from our optical conductivity and XPS measurements. The position of the d_{π} states was inferred from Jiang and Spence's O *K*-edge EELS measurements in addition to our data [38]. A recent *ab initio* study on niobium oxides suggest that a Hubbard *U* of 2 eV on Nb 4*d*

DISTRIBUTION A: Distribution approved for public release

orbitals may be appropriate [39]. Given that recent work has suggested correlation effects are sizeable even in 5*d* transition-metal oxides [40], their contribution in the 4*d* transition-metal oxide NbO_2 needs to be re-examined.

V. SUMMARY

we have reported on the optical conductivity and orbital thermodynamics of NbO_2 films with epitaxial variants deposited on (0001) Al_2O_3. XPS measurements indicate that emission from the occupied $d_{||}$ band states peaks at 1.2 eV below the Fermi level, and O2*p* band edge is ~3.2 eV below the Fermi level. A comparison of the spectral features of NbO_2 and VO_2 states reveals a $d_{||}$-e_g^{π} orbital splitting that is ~0.3 eV larger in NbO_2, which is consistent with its higher MIT temperature. We are able to determine approximate energy separation among Nb 4*d*-like and O2*p*-like electronic states based on experimental data.

TABLE CAPTIONS

Table I. Fitted parameters used to calculate the optical conductivity spectra [Fig. 1(a)-(c)] from spectroscopic ellipsometry. B, C, E, and E_g are in units of eV, while A is dimensionless.

Table II. Core-level binding energies of N2 in eV.

Table III. The 1*s* XPS peak positions in eV of adventitious carbon and oxygen of V1, N1, V2, and the Au and Ag references. Several different Au samples were measured, and the range of C1*s* peak positions is noted.

FIGURE CAPTIONS

FIG. 1. Real optical conductivity σ_1 of (a) V1, (b) N1, and (c) N2, showing the spectra fitted point by point (symbols) as well as by Lorentz and Tauc-Lorentz oscillators (solid lines). The optical conductivity contributions from individual oscillators are shown in the dashed lines. (d) The effective number of electrons n_{eff} involved in optical processes as a function of photon cutoff energy.

FIG. 2. (a) X-ray diffraction 2θ-ω scans and (b) Raman spectra of N1 and N2. The Miller indices used for the NbO_2 peaks refer to its Nb dimerized tetragonal unit cell. The 440 and 222 reflections correspond to the pseudorutile 200 and 101 reflections, respectively.

FIG. 3. (a) Valence band XPS spectrum of V1 and N2, (b) core-level Nb3*d* spectrum of N2, and (c) temperature-dependent electrical transport of N1 and N2.

FIG. 4. Proposed, approximate energy arrangement of electron levels of NbO_2 based on the ordering of orbital states suggested by the theoretical study of Ref. [12] and our measured experimental optical conductivity and valence band XPS features. The position of the d_{π} states was inferred by an EELS study in Ref. [38].

FIG. 5. Ellipsometry data (a) ψ and (b) Δ of N1 taken at two different incident angles. The raw data are shown as open symbols, and fits derived from an oscillator model are shown as lines.

FIG. 6. The spectra of n, k, σ_1, and σ_2 of (a) V1, (b) N1, and (c) N2 attained by oscillator fits.

DISTRIBUTION A: Distribution approved for public release

FIG. 7. (a) The optical conductivity of N1 modeled as a homogenous 54 nm film versus a 52 nm film with an additional 2 nm Nb_2O_5 surface layer attained by point-by-point fits. (b) The optical constants of Nb_2O_5 used in the fitting of (a).

Table I

	Tauc-Lorentz								Lorentz								
	Oscillator 1				Oscillator 2				Oscillator 3			Oscillator 4			Oscillator 5		
	A_1	E_1	C_1	E_{g1}	A_2	E_2	C_2	E_{g2}	A_3	E_3	B_3	A_4	E_4	B_4	A_5	E_5	B_5
V1	5.78	1.31	1.49	0.19	216	3.13	1.00	2.90	8.93	2.92	0.87	2.43	6.53	2.77			
N1	5.63	1.58	1.06	0.41	449	3.95	1.16	3.79	4.20	2.96	1.47						
N2	9.16	1.58	1.08	0.62	223	3.38	1.86	3.30	3.53	2.97	1.17	3.2	4.64	0.72	2.52	5.95	1.97

Table II

	Nb^{5+}	Nb^{4+}	O
$3d_{5/2}$	207.4	205.9	-
$3d_{3/2}$	210.2	208.7	-
1*s*	-	-	530.6

Table III

Sample	C1*s*	O1*s*
Au	284.0-284.4	-
Ag	285.2	-
V1	284.6	529.7
N1	285.3	530.7
N2	285.4	530.6

DISTRIBUTION A: Distribution approved for public release

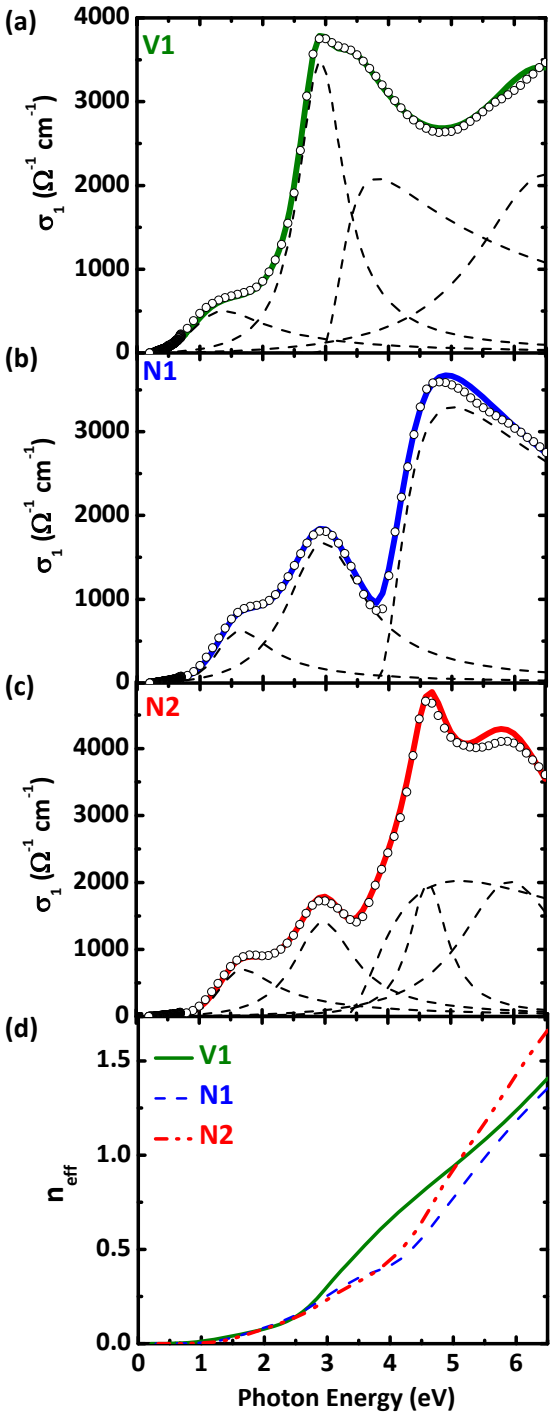

Figure 1

DISTRIBUTION A: Distribution approved for public release

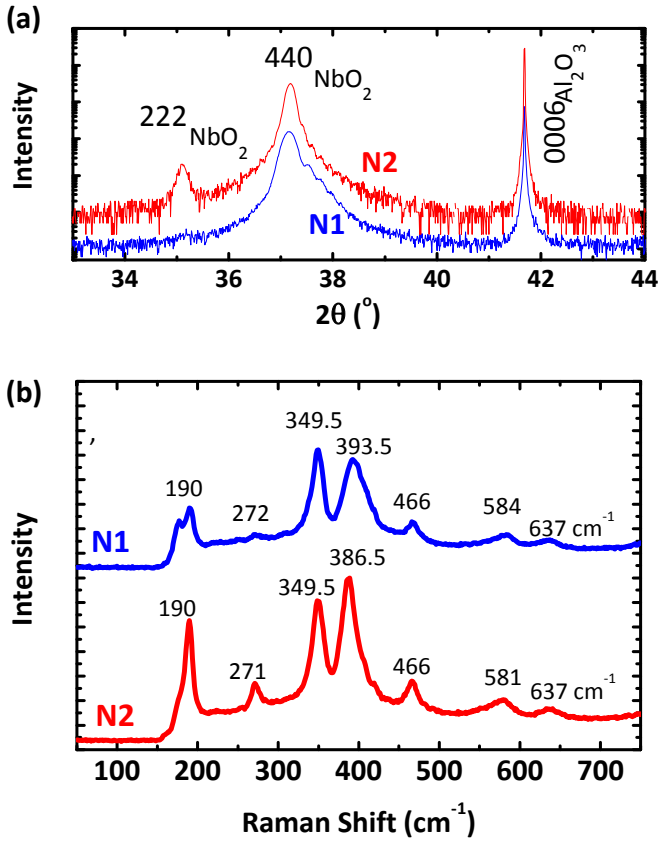

Figure 2

DISTRIBUTION A: Distribution approved for public release

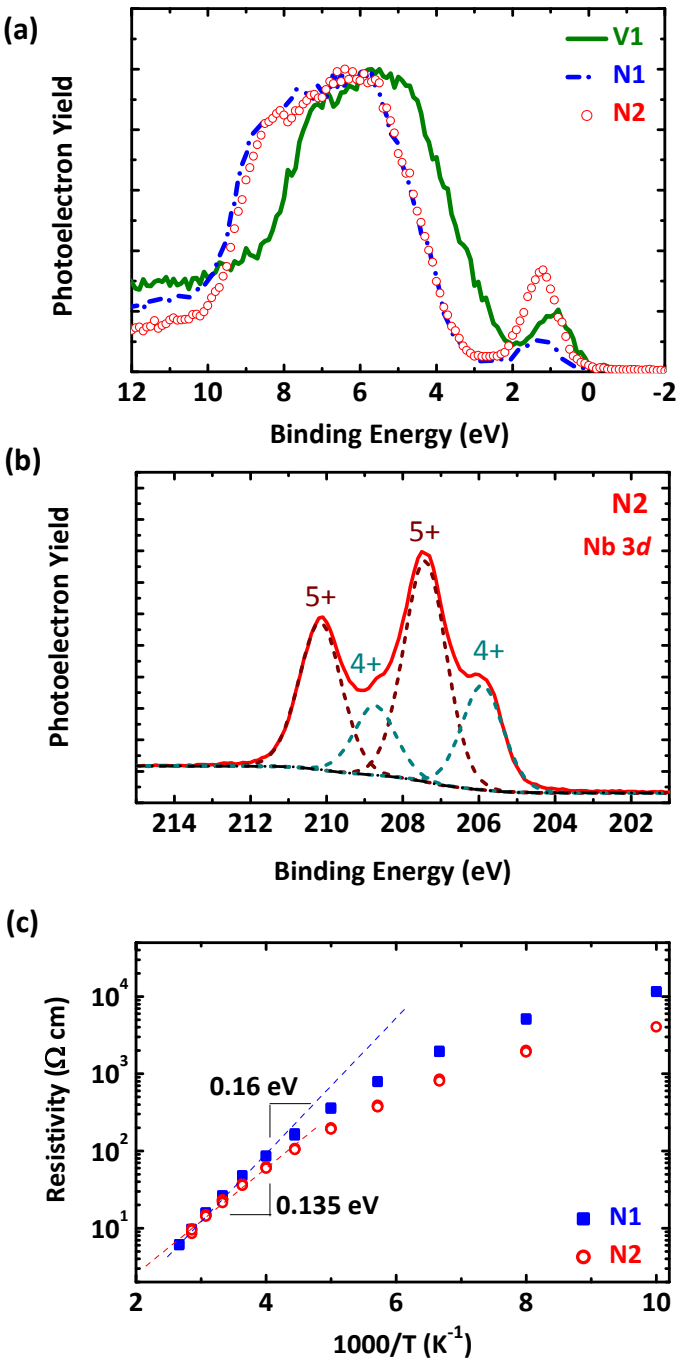

Figure 3

DISTRIBUTION A: Distribution approved for public release

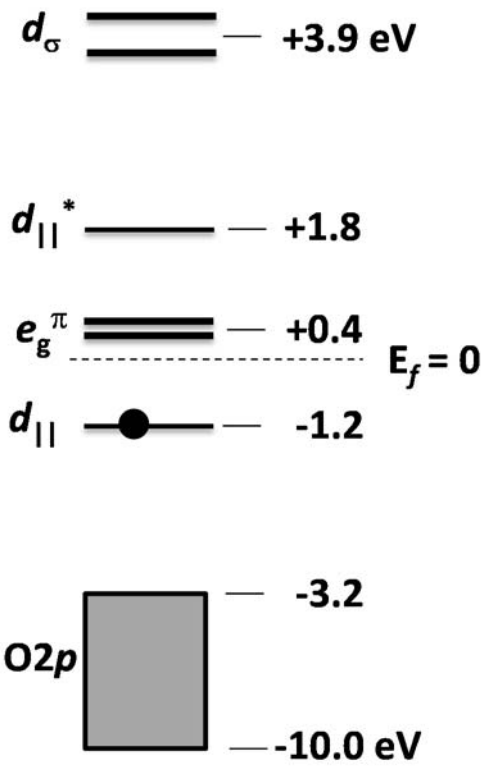

Figure 4

DISTRIBUTION A: Distribution approved for public release

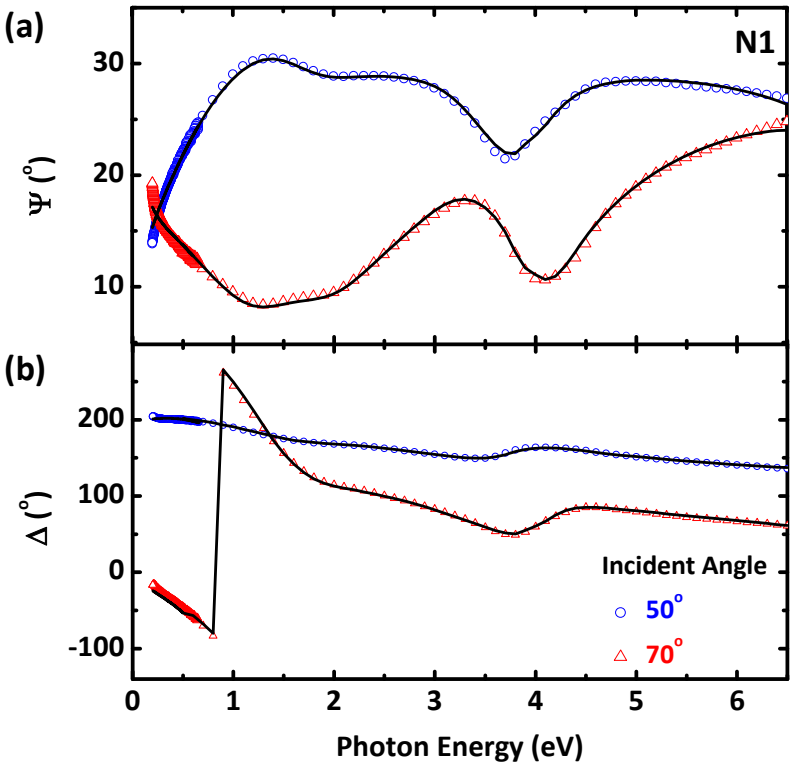

Figure 5

DISTRIBUTION A: Distribution approved for public release

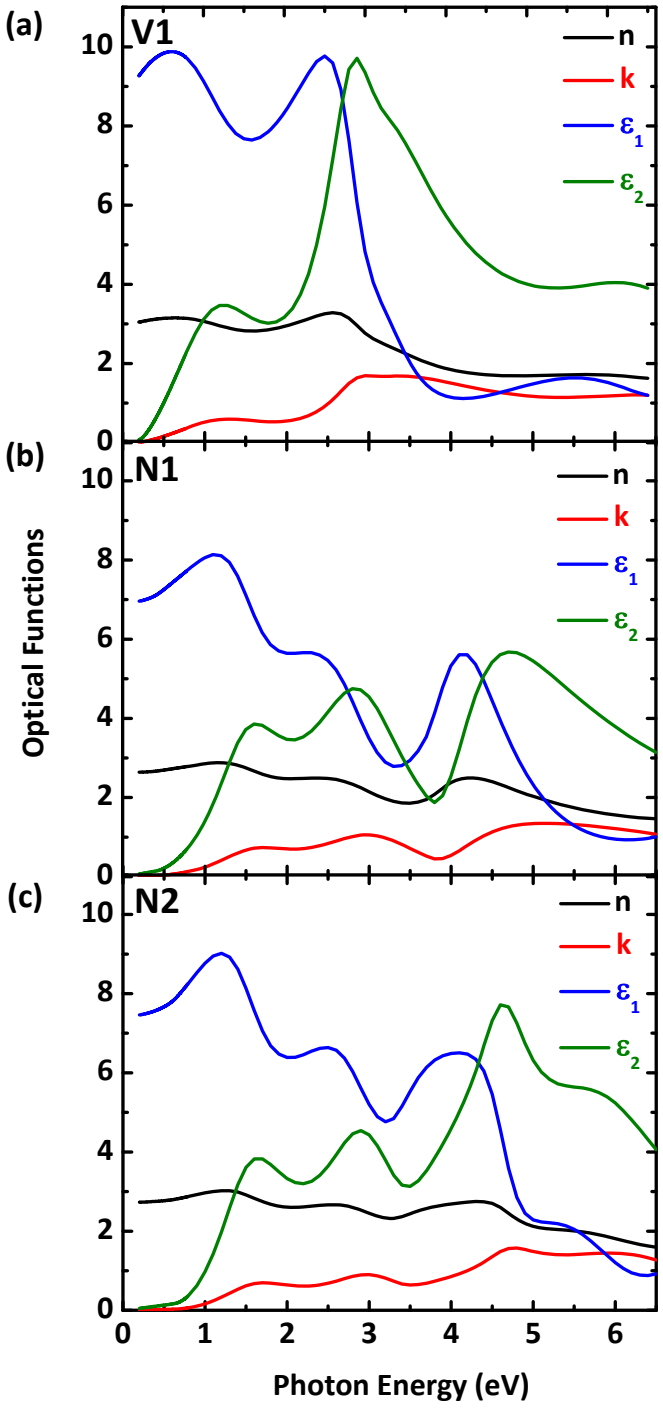

Figure 6

DISTRIBUTION A: Distribution approved for public release

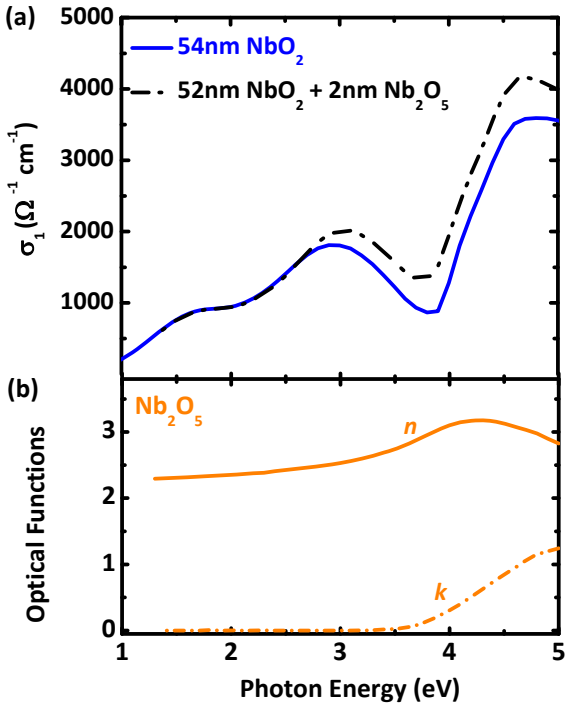

Figure 7

REFERENCES

[1] F. J. Morin, Physical Review Letters **3**, 34 (1959).

[2] S. Biermann, A. Poteryaev, A. I. Lichtenstein, and A. Georges, Physical Review Letters **94**, 4 (2005).

[3] X. Yuan, Y. B. Zhang, T. A. Abtew, P. H. Zhang, and W. Q. Zhang, Physical Review B **86**, 7, 235103 (2012).

[4] C. Weber, D. D. O'Regan, N. D. M. Hine, M. C. Payne, G. Kotliar, and P. B. Littlewood, Physical Review Letters **108**, 5, 256402 (2012).

[5] Z. Y. Zhu and U. Schwingenschlogl, Physical Review B **86**, 4, 075149 (2012).

[6] M. W. Haverkort *et al.*, Physical Review Letters **95**, 4, 196404 (2005).

[7] S. Shin *et al.*, Physical Review B **41**, 4993 (1990).

[8] T. C. Koethe *et al.*, Physical Review Letters **97**, 4, 116402 (2006).

[9] J. Laverock *et al.*, Physical Review B **86**, 5, 195124 (2012).

[10] D. Ruzmetov, S. D. Senanayake, V. Narayanamurti, and S. Ramanathan, Physical Review B **77**, 5, 195442 (2008).

[11] Y. Sakai, N. Tsuda, and T. Sakata, Journal of the Physical Society of Japan **54**, 1514 (1985).

[12] V. Eyert, Europhysics Letters **58**, 851 (2002).

[13] V. Eyert, Physical Review Letters **107**, 4, 016401 (2011).

[14] S. M. Shapiro, J. D. Axe, G. Shirane, and P. M. Raccah, Solid State Communications **15**, 377 (1974).

[15] A. A. Bolzan, C. Fong, B. J. Kennedy, and C. J. Howard, Journal of Solid State Chemistry **113**, 9 (1994).

[16] K. Seta and K. Naito, Journal of Chemical Thermodynamics **14**, 921 (1982).

DISTRIBUTION A: Distribution approved for public release

[17] T. Sakata, K. Sakata, and I. Nishida, Physica Status Solidi **20**, K155 (1967).
[18] R. F. Janninck and D. H. Whitmore, Journal of Physics and Chemistry of Solids **27**, 1183 (1966).
[19] K. Sakata, Journal of the Physical Society of Japan **26**, 867 (1969).
[20] F. J. Wong and S. Ramanathan, Journal of Materials Research **28**, 2555 (2013).
[21] A. B. Posadas, A. O'Hara, S. Rangan, R. A. Bartynski, and A. A. Demkov, Applied Physics Letters **104**, 5, 092901 (2014).
[22] F. J. Wong, Y. Zhou, and S. Ramanathan, Journal of Crystal Growth **364**, 74 (2013).
[23] R. Pynn, J. D. Axe, and R. Thomas, Physical Review B **13**, 2965 (1976).
[24] A. K. Cheetham and C. N. R. Rao, Acta Crystallographica Section B-Structural Science **32**, 1579 (1976).
[25] Y. Zhao, Z. J. Zhang, and Y. H. Lin, Journal of Physics D-Applied Physics **37**, 3392 (2004).
[26] M. K. Bahl, Journal of Physics and Chemistry of Solids **36**, 485 (1975).
[27] R. Fontaine, R. Caillat, L. Feve, and M. J. Guittet, Journal of Electron Spectroscopy and Related Phenomena **10**, 349 (1977).
[28] Goodenou.Jb, Journal of Solid State Chemistry **3**, 490 (1971).
[29] V. Eyert, Annalen Der Physik **11**, 650 (2002).
[30] J. M. Tomczak and S. Biermann, Journal of Physics-Condensed Matter **19**, 12, 365206 (2007).
[31] M. M. Qazilbash, A. A. Schafgans, K. S. Burch, S. J. Yun, B. G. Chae, B. J. Kim, H. T. Kim, and D. N. Basov, Physical Review B **77**, 10, 115121 (2008).
[32] J. M. Tomczak and S. Biermann, Physical Review B **80**, 13, 085117 (2009).
[33] K. Okazaki, S. Sugai, Y. Muraoka, and Z. Hiroi, Physical Review B **73**, 5 (2006).
[34] M. Nazari, Y. Zhao, V. V. Kuryatkov, Z. Y. Fan, A. A. Bernussi, and M. Holtz, Physical Review B **87**, 7, 035142 (2013).
[35] H. W. Verleur, A. S. Barker, and C. N. Berglund, Physical Review **172**, 788 (1968).
[36] W. W. Li, Q. Yu, J. R. Liang, K. Jiang, Z. G. Hu, J. Liu, H. D. Chen, and J. H. Chu, Applied Physics Letters **99**, 3, 241903 (2011).
[37] M. Posternak, A. J. Freeman, and D. E. Ellis, Physical Review B **19**, 6555 (1979).
[38] N. Jiang and J. C. H. Spence, Physical Review B **70**, 7, 245117 (2004).
[39] W. B. Zhang, W. D. Wu, X. M. Wang, X. L. Cheng, D. W. Yan, C. L. Shen, L. P. Peng, Y. Y. Wang, and L. Bai, Surface and Interface Analysis **45**, 1206 (2013).
[40] M. Moretti Sala, K. Ohgushi, A. Al-Zein, Y. Hirata, G. Monaco, and M. Krisch, Physical Review Letters **112** (2014).
[41] J. A. Woollam, B. Johs, C. M. Herzinger, J. Hilfiker, R. Synowicki, and C. L. Bungay, Critical Reviews of Optical Science and Technology **CR72**, 3 (1999).
[42] F. Gervais, in *Handbook of optical constants of solid II*, edited by E. D. Palik (Academic Press, San Diego, 1991), pp. 761.
[43] D. E. Aspnes, Journal of the Optical Society of America **70**, 1275 (1980).
[44] M. P. Seah, L. S. Gilmore, and G. Beamson, Surface and Interface Analysis **26**, 642 (1998).

DISTRIBUTION A: Distribution approved for public release